Early Stage Soliton Observations in the Sulu Sea*

ZACHARY D. TESSLER AND ARNOLD L. GORDON

Lamont-Doherty Earth Observatory, Columbia University, Palisades, New York

CHRISTOPHER R. JACKSON

Global Ocean Associates, Alexandria, Virginia

(Manuscript received 12 September 2011, in final form 25 April 2012)

ABSTRACT

Observations of early stage, large-amplitude, nonlinear internal waves in the Sulu Sea are presented. Water column displacement and velocity profile time series show the passage of two solitary-like waves close to their generation site. Additional observations of the same waves are made as they propagate through the Sulu Sea basin. These waves of depression have an estimated maximum amplitude of 44 m. Observed wave amplitude and background stratification are used to estimate parameters for both a Korteweg–de Vries (K-dV) and a Joseph wave solution. These analytic model solutions are compared with a fully nonlinear model as well. Model wave half-widths bracket the observed wave, with the Joseph model narrower than the K-dV model. The modal structure of the waves change as they transit northward though the Sulu Sea, with higher mode features present in the southern Sulu Sea, which dissipate by the time the waves reach the north. Observed and modeled energies are roughly comparable, with observed potential energy estimated at 6.5×10^7 J m^{-1}, whereas observed kinetic energy is between 4.6×10^7 J m^{-1} and 1.5×10^8 J m^{-1}, depending on the integration limits. If this energy remains in the Sulu Sea, an average dissipation rate of 10^{-9} W kg^{-1} is required over its volume, helping to maintain elevated mixing rates.

1. Introduction

Internal waves at near-tidal frequencies are most often generated by the interaction between tidal motions and ocean boundaries such as continental shelves or shallow sills, which induce perturbations in the water column stratification. At large wave amplitudes, relative to horizontal wavelength, such as those seen in the Sulu Sea by Apel et al. (1985), nonlinear effects become important in the propagation of these perturbations away from the generation site.

Apel and coworkers (Apel et al. 1985; Liu et al. 1985) conducted the first comprehensive study of large-scale internal waves in the Sulu Sea. Over a 2-week period, moored current meter and thermistor chains recorded observations of large, nonlinear internal waves, identified as solitons, at three locations. Solitary internal waves have since been observed throughout the world's seas, both on the continental shelf (Sandstrom and Elliott 1984; New and Pingree 1992; Pan et al. 2007) and in the open ocean (Pinkel 2000; Ramp et al. 2004; Klymak et al. 2006). Indeed, satellite imagery, both synthetic aperture radar (SAR) and optical sun glint, has shown them to be nearly ubiquitous globally (Jackson 2004).

During a March 2009 cruise in the southern Sulu Sea as part of the Philippines Strait Dynamics Experiment (PhilEx), we were in the vicinity of the SS2 mooring location occupied by Apel et al. (1985) in 1980. This is approximately 80 km northeast of the soliton generation site near Pearl Bank in the Sulu Archipelago. From here, waves propagate toward the northwest until they terminate along the southern coast of Palawan Island, where their occurrences have been coupled to harbor seiche activity (Giese et al. 1998).

To our knowledge, these are the first in situ observations of these waves since 1980. Although the larger objective of the PhilEx 2009 cruise was not soliton detection, we took the opportunity of our location and

* Lamont-Doherty Earth Observatory Contribution Number 7544.

Corresponding author address: Zachary D. Tessler, Lamont-Doherty Earth Observatory, 61 Route 9W, Palisades, NY 10964.
E-mail: ztessler@ldeo.columbia.edu

DOI: 10.1175/JPO-D-11-0165.1

© 2012 American Meteorological Society

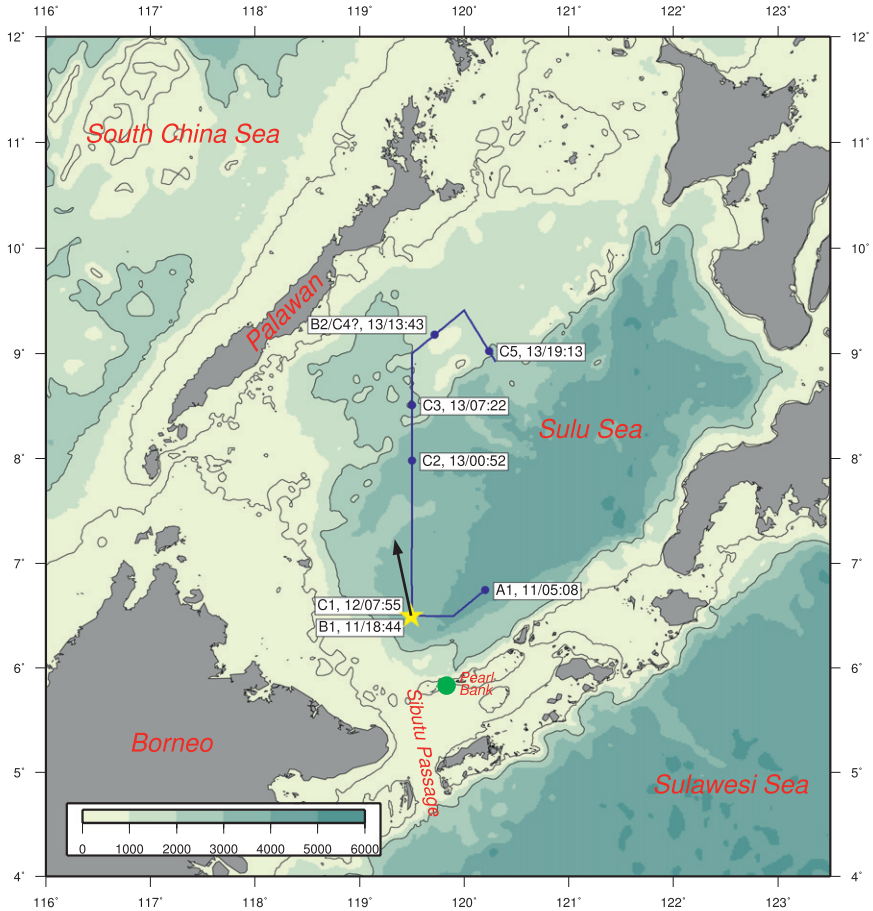

FIG. 1. Study site: The yellow star marks time series location, and blue lines and dots mark ship track and wave crossings. The arrow indicates dominant direction of wave motion, 348°. The green dot marks the approximate soliton generation site. The contour lines are plotted at 100- and 2000-m depths. Timestamps mark the March 2009 date and UTC time of wave crossings, and the wave letter and number correspond with Fig. 7.

timing, during the spring tide when soliton generation is strongest (Apel et al. 1985), to collect a full tidal cycle time series of passing internal waves prior to completing a transect to the north, approximately in line with the soliton ray paths. Additionally, these observations serve as a complement to roughly contemporaneous internal wave studies conducted in other parts of the Philippines (Girton et al. 2011; Jackson et al. 2011).

2. Data

In situ observations of the Sulu Sea solitary waves were made aboard the R/V *Melville* from 11 to 13 March 2009. Data collection consisted of two "regimes". The first was a 25-h stationary observation period on 11–12 March, at 6.5°N, 119.5°E, using hull-mounted acoustic Doppler current profilers (ADCPs) and a conductivity–temperature–depth (CTD) package at midthermocline depth, bracketed by two full-depth CTD profiles. The CTD was located at midthermocline depth for approximately 16 h, between the profiles, where the vertical temperature gradient is greatest to best resolve vertical water displacements associated with the passage of the wave.

In the second regime, we collected underway hull-mounted ADCP and sea surface measurements along a northward cruise track through the Sulu Sea on 12–13 March. The cruise track and time series location are shown in Fig. 1. The hull-mounted ADCP system consisted of two RDI Ocean Surveyor instruments, operating at 75 (OS75) and 150 kHz (OS150). Because of the superior depth penetration, approximately 600 m with a configured bin size of 8 m, most of the data used in this study are from the OS75 instrument.

3. Wave observations

Water column displacement associated with wave passage is estimated from the temperature time series

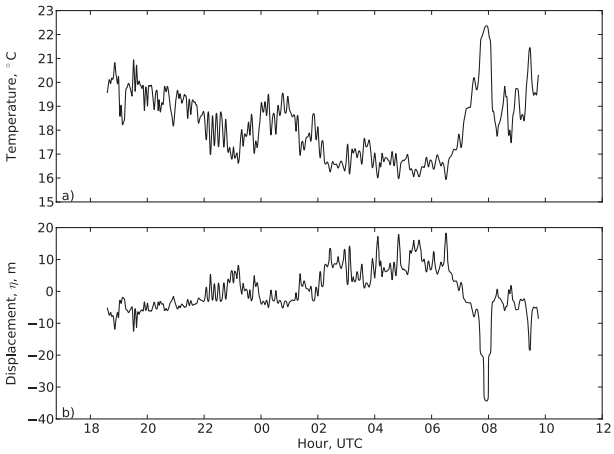

FIG. 2. (a) Potential temperature during CTD time series, adjusted to compensate for CTD package depth changes using a linear approximation around 154 dbar based on the background temperature profile. A 250-s low-pass filter was used to remove high-frequency internal wave signatures. (b) Estimated water column displacement of the $\theta = 17.86°C$ isopycnal, found at 154 dbar in the background temperature profile.

shown in Fig. 2a. After filtering to remove high-frequency internal wave signatures, we assume all remaining temporal temperature variability is due to vertical displacement of the water column, rather than temperature changes due to horizontal advection. This assumption is met in the Sulu Sea, where $w(dT/dz) \gg u(dT/dx)$. Figure 2b shows the estimated displacement time series of a representative isotherm in the thermocline.

Displacement is estimated by mapping the observed temperature at the CTD with its depth in the background temperature profile (Fig. 3). The zero displacement depth was taken as the mean source depth of the observed water. There is a level of ambiguity in defining the zero displacement depth given the relatively short deployment, which has the effect of biasing the observed wave amplitude small. An alternative method, taking the mean displacement in the 6 h preceding the wave's arrival, results in a wave amplitude approximately 6 m greater. The vertical structure of the water column displacement due to wave passage is assumed to have the shape of the first normal mode w_1, consistent with the findings of Apel et al. (1985) and velocity structure results.

Velocity structure

Hull-mounted ADCP data were rotated into the direction of wave propagation, determined through a filtering and regression procedure. Data were high-pass filtered using a 3-h Hanning window to remove low-frequency background motion. The dominant direction of mean wave motion in the upper 100 m was found using a linear orthogonal regression constrained at the origin, minimizing the residuals associated with a coordinate axes rotation. Relative to true north, wave motion was oriented at 348° and 346° for the OS75 and OS150 instruments, respectively. This direction was insensitive to the filter length or the maximum depth included in the flow average.

Rotated OS75 ADCP data collected during the CTD time series are shown in Figs. 4 and 5. Two wave packets were observed during this CTD deployment, B1 and C1; A1 was observed while underway prior to the CTD profiles. Packet B1 was relatively weak and less well defined, with the wave crest passing at 1850 UTC 11 March. The first crest of the second packet, C1, stronger and better defined than the first, passed at 0800 UTC 12 March, followed by an additional five weaker crests. The arrival of the wave was characterized by positive along-axis horizontal motion in the upper 150 m of the water column, with out of phase motion below. There was little transverse wave motion. Downward vertical motion was observed with the arrival of the wave, on the order of 1–3 cm s^{-1}. The transition from positive to negative horizontal wave motion is coincident with upward vertical motion of similar strength. For additional insight into the wave's structure, we compare the normal mode oscillations to observed motions by calculating a set of empirical orthogonal functions (EOFs) and their associated principal components (PCs) from high-pass-filtered transect ADCP data (Fig. 6). The inverted data matrix consisted of OS75 data from the full northward Sulu Sea transect, high-pass filtered using a 3-h Hanning window, with the temporal mean at each depth removed.

The first three EOFs are broadly consistent with the horizontal motions associated with the first three normal modes. The arrival of the near-surface pulse is associated with strong responses in both the first and second EOFs (Fig. 5c), whereas later crests are predominately associated with variability in the second EOF. Together, these two modes result in the sign change near 200 m, shallower than the first normal mode maximum at 537 m. Above roughly 150 m, both modes add constructively, whereas below 200 m the first EOF becomes small and the second becomes strongly negative. The first EOF, similar in shape to the first normal mode, is seen to peak with each of the subsequent wave crossings during the transect (Fig. 7).

However, the second EOF response to this wave, C1, is dissimilar to later wave observations, where we do not observe any particular response to stand out above the noise level. This suggests that either this higher mode response dissipates as the wave develops and travels through the Sulu Sea or the underway crossings later in the transect were inadequate to fully observe the wave structure. We thus use the first PC response to help

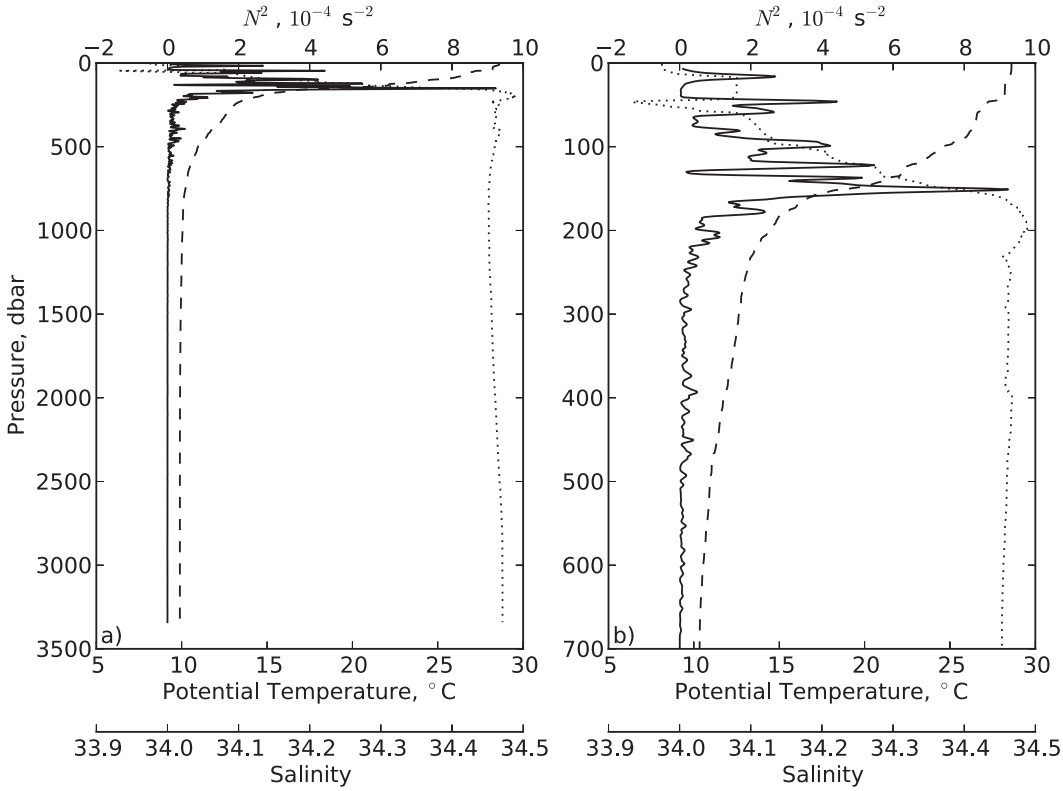

FIG. 3. Stratification at the time series site. The solid line is buoyancy frequency, the dashed line is potential temperature, and the dotted line is salinity.

identify soliton passage during the Sulu Sea transect, where only ADCP data are available.

On the northward transect along 119.5°E, internal wave packets were observed several more times, both visually (see Jackson et al. 2011, Fig. 2b) and in the ADCP record. Given the historical wave speeds of Apel et al. (1985), theoretical speeds discussed below, and an empirical model of internal wave propagation based on satellite imagery (Jackson 2009), it is believed wave C1 was encountered at least three more times during the ship transit. These wave crossings during the Sulu Sea transect are identified in Fig. 7. The first principal component of the along-axis, high-pass-filtered OS150 data responds increasingly strongly to later wave crossings, before weakening dramatically near the shallower regions of the northern Sulu Sea. This also suggests that the first mode gains energy during the wave's development, likely from the background tide, while the higher mode motions weaken. During the transect, other ship operations were ongoing, primarily CTD casts. Because of the stop-and-go nature of that work, in a number of cases we "leapfrogged" the same wave multiple times or observed only the leading or trailing edge of the wave, presenting difficulties in fully analyzing these wave crossings.

4. Discussion

a. Model comparison

Wave C1 was observed with a half-width $L \approx 3400$ m. Given the thermocline thickness $h \approx 200$ m and the full ocean depth $H \approx 3300$ m, these scales suggest the finite-depth theory developed by Joseph (1977) and Kubota et al. (1978) is the most appropriate analytic, weakly nonlinear (WNL) model for this site. For comparison, we also calculate the commonly used Korteweg–de Vries (K-dV) shallow-water model (Korteweg and de Vries 1895). Past work has shown that the K-dV fit to laboratory observations can be better than the Joseph model, despite the strict scaling regimes of each theory (Koop and Butler 1981; Segur and Hammack 1982; Kao et al. 1985). These weakly nonlinear analytic models are also compared with the results of a fully nonlinear (FNL) numerical model, which solves the Dubreil–Jacotin–Long equation, finding the isopycnal displacements that minimize the potential energy for a specified available potential energy (APE; Turkington et al. 1991; Stastna and Lamb 2002). This model was run in an iterative manner to calculate waves with maximum isopycnal displacements matching those described above.

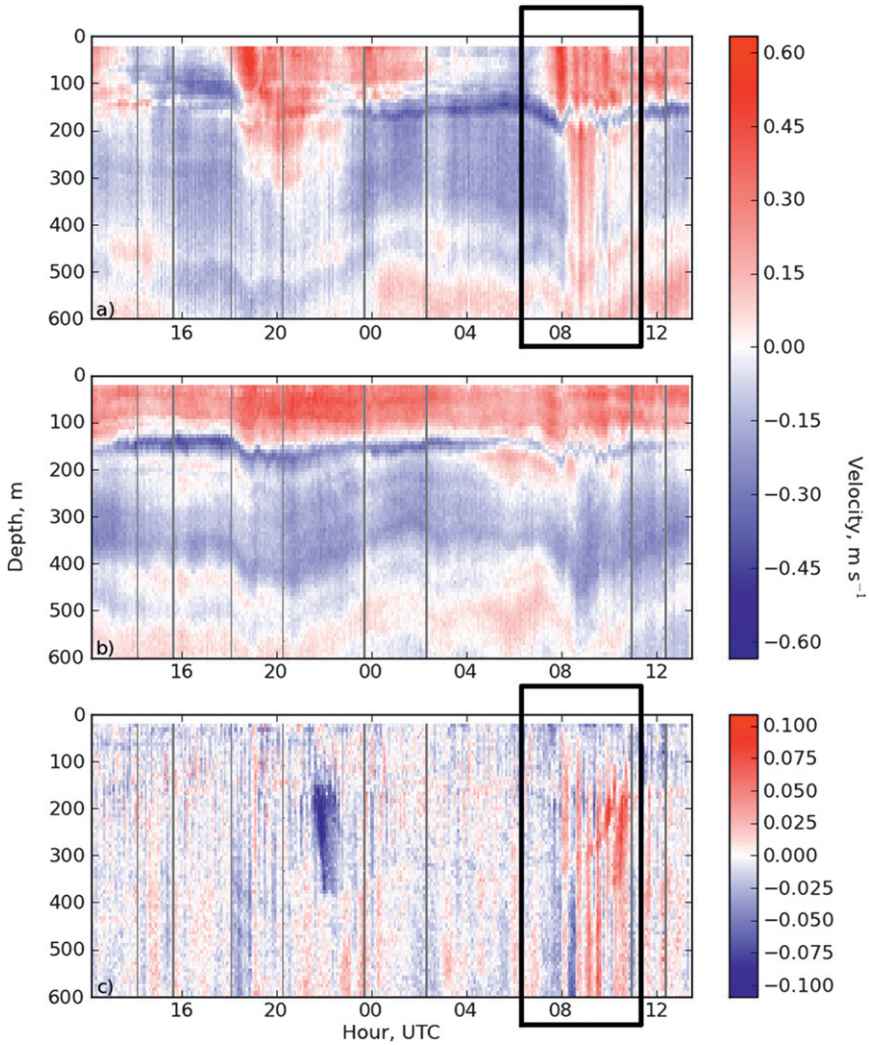

FIG. 4. Velocity structure during time series, from the OS75 ADCP, on 11–12 Mar 2009. (a) Along-axis flow, (b) transverse flow, and (c) vertical flow, where panels (a) and (b) share a common color scale. Horizontal wave motions are oriented at 348° relative to true north. Strong vertical motions at 2200 UTC 11 Mar and 1000 UTC 12 Mar between 150 and 400 m are spurious signals related to diurnal migration of scatters in the water column. Wave-induced vertical motions have magnitudes between 0.01 and 0.05 m s^{-1}. Boxes indicate data shown in Fig. 5.

1) JOSEPH MODEL

The Joseph equation steady-state solitary wave solution, using the notation of Apel et al. (1985), is

$$\eta(\xi) = \frac{-\eta_0}{\cosh^2(a\xi) + \sinh^2(a\xi)/(a^2b^2)}, \qquad (1)$$

where $\xi = x - ct$, $b = 4\beta c_0/\alpha\eta_0$, and a is a solution to $ab\tan(aH) = 1$. The environmental parameters α and β, measures of nonlinearity and dispersion, respectively, are functions of the first normal mode w_1 and of H. The nonlinearity parameter α also depends on the long-wavelength linear wave speed $c_0 = c_1(1 - \beta/H)$, where c_1 is the eigenvalue associated with w_1. The nonlinear soliton wave speed c is given by

$$c = c_0\left[\frac{\beta}{H}(1 - \delta\cot\delta) + 1\right], \qquad (2)$$

where $\delta = 2aH$.

2) K-DV MODEL

The steady-state solution to the K-dV equation takes the form

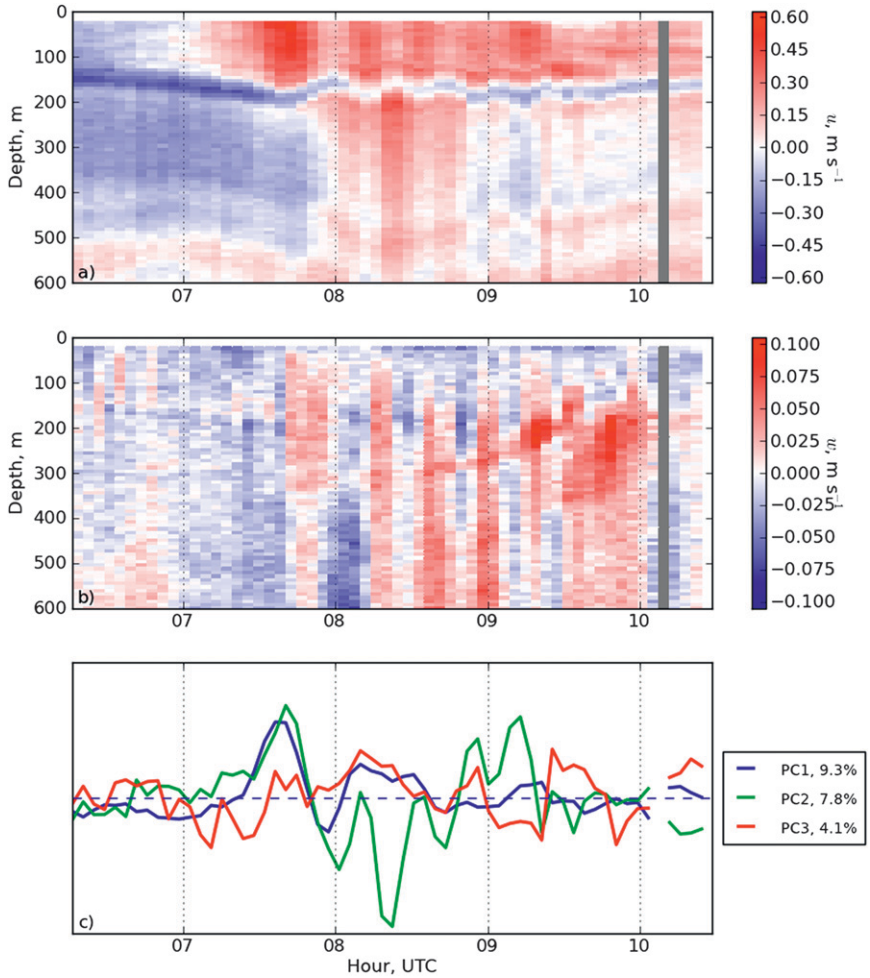

FIG. 5. Velocity structure during passage of wave C1, from the OS75 ADCP, on 12 Mar 2009. (a) Along-axis flow, (b) vertical flow, and (c) the first three PCs. PC colors correspond with the associated EOFs in Fig. 6b.

$$\eta(\xi) = -\eta_0 \operatorname{sech}^2(\xi/\Delta) \tag{3}$$

where $\xi = x - ct$, $c = c_1 + \alpha\eta_0/3$, and $\Delta = \sqrt{12\beta/\alpha\eta_0}$. The environmental parameters α and β, given by Ostrovsky and Stepanyants (1989), take a slightly different form than in the Joseph model.

The parameters α and β for the two models are calculated using the background stratification observed prior to the CTD time series and the resulting first normal mode structure w_1 and linear perturbation speed c_1. Using the estimated isopycnal displacement field described above, we calculate the maximum wave displacement η_0 = 43.5 m at depth z_0 = 537 m for wave C1. Wave amplitudes at other depths are scaled by w_1. The two modeled waveforms are shown in Fig. 8. The model fit is sensitive to η_0, though our estimated value of η_0 compares reasonably with that observed by Apel et al. (1985) of $\eta_0 \approx 50$ m. Relevant parameter values are shown in Table 1.

Given the noise in the observed isopycnal displacement, it is difficult to identify either model as clearly superior. The residual differences between the observed and modeled waves show the K-dV model residuals to be marginally smaller than the Joseph model on the leading edge of the wave, with opposite results on the trailing edge. This result is consistent with small differences in the modeled wave widths and the asymmetry between the observed leading and trailing edges, likely due to the influence of the trailing waves not included in the steady-state solitary wave models. In time coordinates, we find the full width at half maximum amplitude (FWHM) of 23.0 min falls between that for the K-dV model, 26.3 min, and the Joseph model, 16.7 min. The FNL model FWHM falls between the two analytic models.

Observed wave speed between observations C1 and C3 was approximately 2.55 m s^{-1}. This compares well with the Joseph model nonlinear velocity of 2.57 m s^{-1} at the

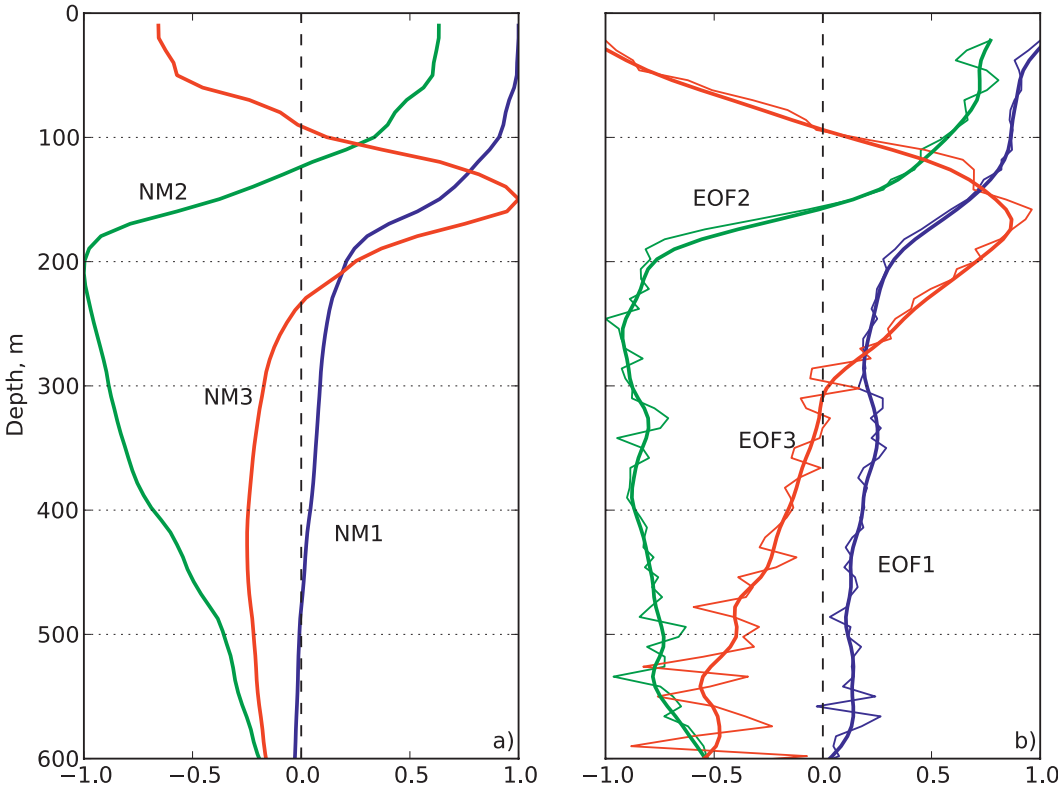

FIG. 6. (a) Normal modes and (b) EOFs, calculated from high-pass-filtered transect OS75 ADCP data. EOF colors correspond with their associated PCs in Fig. 5c. EOF smoothing is done using a 10-dbar-scale filter.

time series site but is slower than the K-dV model velocity of 2.69 m s^{-1}. The FNL model phase speed is 2.54 m s^{-1}, very close to the observed speed. Small differences between the average wave speed through the Sulu Sea and the modeled velocities at the time series site are expected because of changes in water depth and stratification. Effects of background shear are likely to be small, less than 5% for first mode waves (Apel et al. 1985).

Modeled velocities are calculated, assuming no cross-axis currents and zero background flow, from

$$w = \frac{\partial \eta}{\partial t} \quad \text{and} \tag{4}$$

$$\frac{\partial u}{\partial x} = -\frac{\partial w}{\partial z}, \tag{5}$$

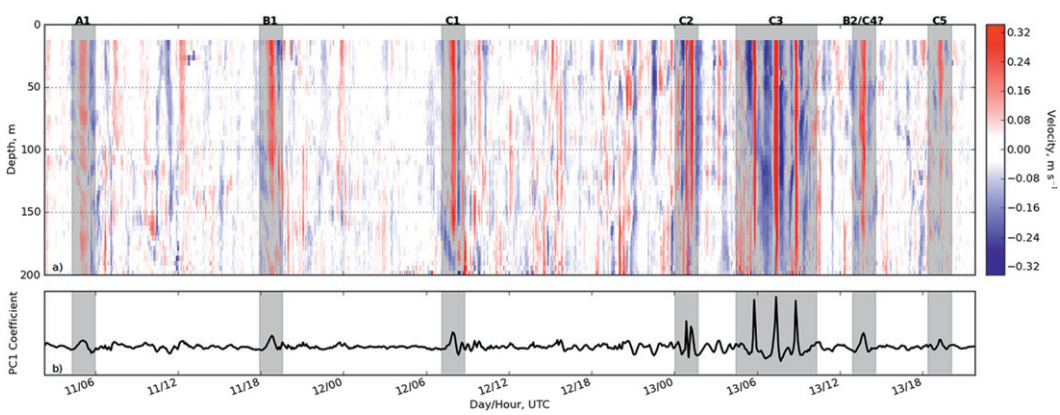

FIG. 7. (a) The 2-h high-pass-filtered OS150 ADCP time series during the Sulu Sea transect and (b) the first PC. This EOF contains 25% of the variance in the filtered time series.

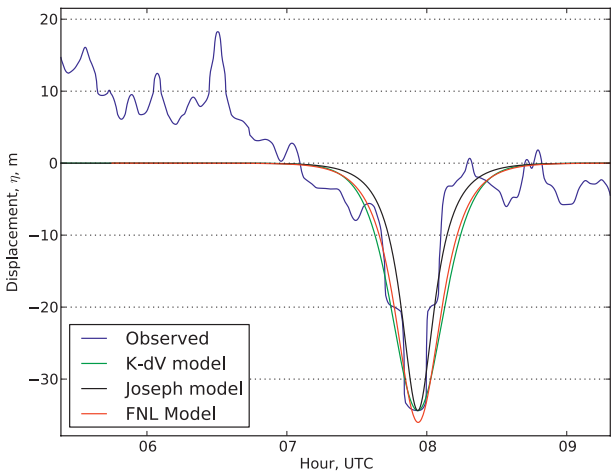

FIG. 8. (a) Estimated observed displacement η of the isotherm observed at a depth of 150 m during the full water column profile (blue). The two WNL soliton models are scaled to the maximum displacement of this isotherm assuming a first mode vertical structure. There are no vertical structure assumptions in the FNL model.

and are compared with observed velocities in Fig. 9. We find that both the WNL and FNL modeled horizontal velocity structure through the wave crest agree well with the observations. Near-surface velocities are approximately 60 cm s^{-1}, dropping to close to zero by 200-m depth. Deeper velocities are in poorer agreement, with the observed flow opposing the surface current more strongly than the models predict. Additionally, the zero crossing is observed to be about 100 m higher than predicted by the FNL model and about 300 m higher than the WNL K-dV model, even when accounting for the narrow background shear layer observed near 200 m.

Vertical velocities are in poorer agreement, not surprisingly, given the greater difficulty in observing the much smaller vertical velocities than horizontal in the ocean. Observed peak vertical velocities associated with the wave passage are roughly 50%–75% of the modeled velocities. Additionally, the diurnal migration of scatters introduces a spurious vertical velocity, which we attempt to remove using a daily composite of vertical velocity in the Sulu Sea (Plueddemann and Pinkel 1989). This composite consists of approximately 4 days of Sulu Sea data. Visual inspection confirms that the diurnal mean vertical velocity is dominated by the migration of scatters.

b. Wave energetics

Estimates of potential energy and kinetic energy (KE) can be made from the wave ADCP and CTD observations during the time series, as well as from the models. Because of the limited depth penetration of the hull-mounted ADCP, we first estimate the proportion of depth-integrated kinetic energy that is within its 614-m range. Assuming the distribution of kinetic energy associated with the soliton takes the shape of the first normal mode w_1 and its associated horizontal motions u_1, we calculate two scaling factors for horizontal and vertical motion, κ and λ, representing the reciprocal of the proportion of kinetic energy in the upper 614 m of the normal mode oscillations.

Using the scaling factors to extrapolate from the upper ocean observed by the ADCP to full ocean depth, we calculate the kinetic energy,

$$\mathrm{KE} = \frac{1}{2}\rho_0 \int_{x_1}^{x_2}\int_{-614\,m}^{0} \kappa u(t,z)^2 + \kappa v(t,z)^2 + \lambda w(t,z)^2 \, dz\, dx, \tag{6}$$

where u, v, and w are first 3-h high-pass filtered to remove background currents. For the model estimates of kinetic energy, we integrate over the full domain, with $\kappa = \lambda = 1$.

The total observed kinetic energy contained in the full solitary wave is sensitive to the integration limits and additionally complicated by the wave train following the first large wave. Integrating from 5 km on the leading edge of the wave, approximately where the energy rises above the background values on the order of 2 kJ m^{-2} to 2.3 km on the trailing edge where the kinetic energy begins to rise in a new oscillation, we calculate a total kinetic energy of $\mathrm{KE}_{\mathrm{Obs}} = 47$ MJ m^{-1}. It is also instructive to calculate the kinetic energy within broader integration limits, because the background tide contains additional kinetic energy, some of which likely contributes to the growth of the leading wave as the wave develops. Because

TABLE 1. Observed wave and modeled wave parameters. Phase speed c refers to the observed speed between crossings and the nonlinear phase speed for each model.

	η_0 (m)	α (s^{-1})	β ($m^3\ s^{-1}$)	c (m s^{-1})	FWHM (m)	KE (J m^{-1})	APE (J m^{-1})
Obs	44			2.55	3.5×10^3	$4.7 - 15 \times 10^7$	6.5×10^7
K-dV	44	1.7×10^{-2}	3.7×10^5	2.69	4.2×10^3	1.1×10^8	4.8×10^7
Joseph	44	1.7×10^{-2}	1.1×10^2	2.57	2.5×10^3	6.6×10^7	2.9×10^7
FNL	44			2.54	3.0×10^3	9.1×10^7	8.4×10^7

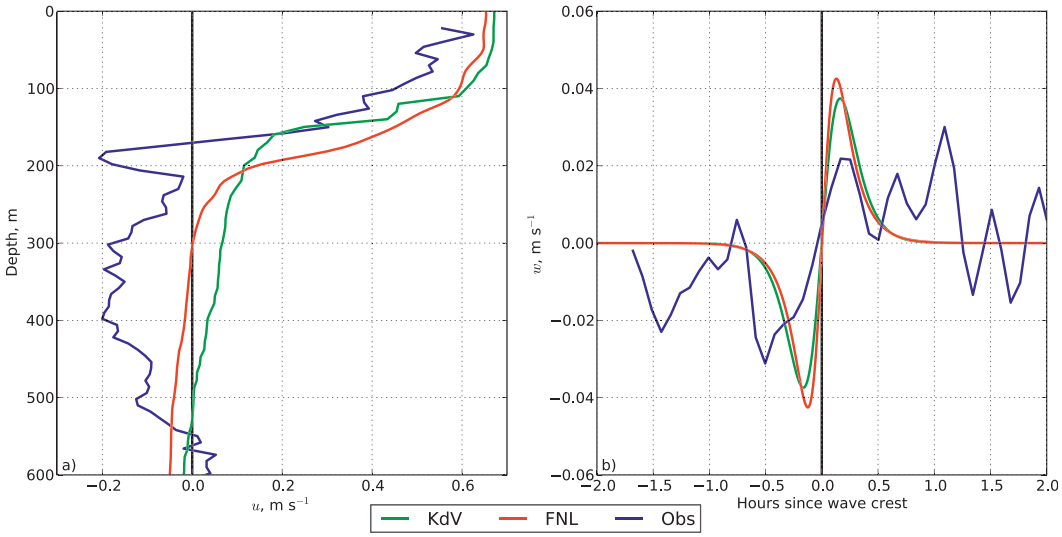

FIG. 9. (a) Vertical profiles of along-axis horizontal velocity u through the wave crest and (b) time series of vertical velocity at the depth of maximum mean vertical velocity magnitude. The vertical velocities are shown at the depth of maximum vertical motion. For the WNL K-dV model, this is at the depth of the first normal mode maximum, 537 m. For the FNL model, this is at 302 m. For the observed motions, we use the FNL model depth.

we expect the leading wave to grow as it transits northward throughout the Sulu Sea, this provides a sense of the extent of that growth. Integrating from 10 km prior to the first wave crest to 25 km after and vertically through the water column, we find $KE_{Obs} = 148$ MJ m^{-1} of kinetic energy. Modeled kinetic energies, calculated from the estimated u and w velocities throughout the domain, are all within this range, with the FNL model between the K-dV and Joseph models (Table 1).

Available potential energy is calculated as the difference between the total potential energy in the domain during wave passage and a suitable background rest state potential energy,

$$\mathrm{APE} = g\int_{-L/2}^{L/2}\int_{-H}^{0}(\rho - \overline{\rho})z\,dz\,dx. \qquad (7)$$

Here, $\rho(t, z)$ is taken alternatively as the estimated observed density during wave passage or the density field obtained by perturbing the background density with the modeled waveforms, and $\overline{\rho}(z)$ is the estimated background density profile.

To determine this background state, we follow the method of Hebert (1988) and Winters et al. (1995), where the density in the domain is adiabatically redistributed, in a water-parcel sense, into the lowest potential energy state with horizontal isopycnals. This redistribution of density is sensitive to the chosen domain limits. Following Klymak et al. (2006), we calculate the APE over a range of domains and find convergence when the domain is greater than about 10 wavelengths.

Applying this procedure to the estimated density field during the waves passage, we calculated $APE_{Obs} = 65$ MJ m^{-1}. Applying the modeled K-dV and Joseph (Jos) waveforms to the background density field, we find $APE_{K\text{-}dV} = 48$ MJ m^{-1}, whereas $APE_{Jos} = 29$ MJ m^{-1}. The peak available potential energy density is approximately an order of magnitude greater than waves observed elsewhere in the Philippine Archipelago (Girton et al. 2011).

Of note is that the observed kinetic energy estimate here is based fully on ADCP data and is sensitive to chosen integration limits. Additionally, the models used for the energy estimates assume the wave is fully formed and solitary at this site. The single crest KE_{Obs} estimate is lower than that predicted by the solitary wave models for a wave of its amplitude, whereas the broader integration appears to include some energy that remains outside the leading crest.

The energy contained in these waves must dissipate in transit either through turbulence or generation of small-amplitude internal waves or upon shoaling and breaking near Palawan Island. Given that the waves are dominated by first mode motions and they maintain their shape through much of the Sulu Sea, most of the energy is likely to be transported to the northwest Sulu Sea. Taking the total wave energy $E = \mathrm{KE} + \mathrm{APE}$ as approximately 2×10^8 J m^{-1}; crest lengths of roughly 100 km; and one to two waves per day, depending on the tidal cycle (Apel et al. 1985), these waves carry on the order of 5×10^8 W toward Palawan. If all this energy is dissipated locally (i.e., within the 4.3×10^{14} m^3 Sulu Sea), we find a bulk dissipation rate on the order of 10^{-9} W kg^{-1}, similar to

average oceanic background dissipation rates (Toole et al. 1994; Kunze et al. 2006). Along with additional input from wind (Pullen et al. 2008), from the internal tide, and at the Sulu Sea boundaries, this energy likely contributes to maintaining the elevated mixing rates observed previously in the Sulu Sea (Tessler et al. 2010).

The observations of early state solitary waves in the southern Sulu Sea presented in this paper support and extend the data collected by Apel et al. (1985) near their mooring site SS2. We collected CTD and hull-mounted ADCP time series data, estimated idealized waveforms based on the K-dV and Joseph soliton models, and compared these with a fully nonlinear model. At this site, the models are broadly consistent with the observed wave structure. Additional velocity and CTD time series observations in the northern Sulu Sea would allow estimates of energy dissipation and insights into the propagation and evolution of these waves.

Acknowledgments. This work was supported by the Office of Naval Research Grant N00014-09-1-0582 to Lamont-Doherty Earth Observatory of Columbia University and a National Defense Science and Engineering Graduate Fellowship. The authors thank the captain and crew of the R/V *Melville* for their support at sea. Thanks go to Jody Klymak, Andreas Thurnherr, and two anonymous referees for their helpful comments. Kevin Lamb graciously provided code and assistance with the nonlinear modeling.

REFERENCES

Apel, J. R., J. R. Holbrook, A. K. Liu, and J. J. Tsai, 1985: The Sulu Sea internal soliton experiment. *J. Phys. Oceanogr.,* **15,** 1625–1651.

Giese, G. S., D. C. Chapman, M. G. Collins, R. Encarnacion, and G. Jacinto, 1998: The coupling between harbor seiches at Palawan Island and Sulu Sea internal solitons. *J. Phys. Oceanogr.,* **28,** 2418–2426.

Girton, J. B., B. S. Chinn, and M. H. Alford, 2011: Internal wave climates of the Philippine Seas. *Oceanography,* **24,** 100–111, doi:10.5670/oceanog.2011.07.

Hebert, D., 1988: The available potential energy of an isolated feature. *J. Geophys. Res.,* **93** (C1), 556–564.

Jackson, C. R., 2004: An atlas of internal solitary-like waves and their properties. 2nd ed. Global Ocean Associates Tech. Rep., 560 pp. [Available online at http://www.internalwaveatlas.com/Atlas2_index.html.]

——, 2009: An empirical model for estimating the geographic location of nonlinear internal solitary waves. *J. Atmos. Oceanic Technol.,* **26,** 2243–2255.

——, Y. Arvelyna, and I. Asanuma, 2011: High-frequency nonlinear internal waves around the Philippines. *Oceanography,* **24,** 90–99, doi:10.5670/oceanog.2011.06.

Joseph, R. I., 1977: Solitary waves in a finite depth fluid. *J. Phys.,* **225A,** 10–13.

Kao, T. W., F. S. Pan, and D. Renouard, 1985: Internal solitons on the pycnocline: Generation, propagation, and shoaling and breaking over a slope. *J. Fluid Mech.,* **159,** 19–53, doi:10.1017/S0022112085003081.

Klymak, J. M., R. Pinkel, C.-T. Liu, A. K. Liu, and L. David, 2006: Prototypical solitons in the South China Sea. *Geophys. Res. Lett.,* **33,** L11607, doi:10.1029/2006GL025932.

Koop, C. G., and G. Butler, 1981: An investigation of internal solitary waves in a two-fluid system. *J. Fluid Mech.,* **112,** 225–251, doi:10.1017/S0022112081000372.

Korteweg, D. J., and G. de Vries, 1895: On the change of form of long waves advancing in a rectangular canal, and on a new type of stationary waves. *Philos. Mag.,* **39,** 422–443.

Kubota, T., D. R. S. Ko, and L. D. Dobbs, 1978: Weakly-nonlinear, long internal gravity waves in stratified fluids of finite depth. *J. Hydronaut.,* **12,** 157–165.

Kunze, E., E. Firing, J. M. Hummon, T. K. Chereskin, and A. M. Thurnherr, 2006: Global abyssal mixing inferred from lowered ADCP shear and CTD strain profiles. *J. Phys. Oceanogr.,* **36,** 1553–1576.

Liu, A. K., J. R. Holbrook, and J. R. Apel, 1985: Nonlinear internal wave evolution in the Sulu Sea. *J. Phys. Oceanogr.,* **15,** 1613–1624.

New, A. L., and R. D. Pingree, 1992: Local generation of internal soliton packets in the central Bay of Biscay. *Deep-Sea Res.,* **39A,** 1521–1534, doi:10.1016/0198-0149(92)90045-U.

Ostrovsky, L. A., and Yu. A. Stepanyants, 1989: Do internal solitons exist in the ocean? *Rev. Geophys.,* **27,** 293–310.

Pan, J., D. A. Jay, and P. M. Orton, 2007: Analyses of internal solitary waves generated at the Columbia River plume front using SAR imagery. *J. Geophys. Res.,* **112,** C07014, doi:10.1029/2006JC003688.

Pinkel, R., 2000: Internal solitary waves in the warm pool of the western equatorial Pacific. *J. Phys. Oceanogr.,* **30,** 2906–2926.

Plueddemann, A. J., and R. Pinkel, 1989: Characterization of the patterns of diel migration using a Doppler sonar. *Deep-Sea Res.,* **36A,** 509–530, doi:10.1016/0198-0149(89)90003-4.

Pullen, J., J. D. Doyle, P. May, C. Chavanne, P. Flament, and R. A. Arnone, 2008: Monsoon surges trigger oceanic eddy formation and propagation in the lee of the Philippine Islands. *Geophys. Res. Lett.,* **35,** L07604, doi:10.1029/2007GL033109.

Ramp, S. R., and Coauthors, 2004: Internal solitons in the northeastern South China Sea Part I: Sources and deep water propagation. *IEEE J. Oceanic Eng.,* **29,** 1157–1181, doi:10.1109/JOE.2004.840839.

Sandstrom, H., and J. A. Elliott, 1984: Internal tide and solitons on the Scotian shelf: A nutrient pump at work. *J. Geophys. Res.,* **89** (C4), 6415–6426.

Segur, H., and J. L. Hammack, 1982: Soliton models of long internal waves. *J. Fluid Mech.,* **118,** 285–304, doi:10.1017/S0022112082001086.

Stastna, M., and K. G. Lamb, 2002: Large fully nonlinear internal solitary waves: The effect of background current. *Phys. Fluids,* **14,** 2987–2999.

Tessler, Z. D., A. L. Gordon, L. J. Pratt, and J. Sprintall, 2010: Transport and dynamics of the Panay Sill overflow in the Philippine Seas. *J. Phys. Oceanogr.,* **40,** 2679–2695.

Toole, J. M., K. L. Polzin, and R. W. Schmitt, 1994: Estimates of diapycnal mixing in the abyssal ocean. *Science,* **264,** 1120–1123.

Turkington, B., A. Eydeland, and S. Wang, 1991: A computational method for solitary internal waves in a continuously stratified fluid. *Stud. Appl. Math.,* **85,** 93–127.

Winters, K. B., P. N. Lombard, J. J. Riley, and E. A. D'Asaro, 1995: Available potential energy and mixing in density stratified fluids. *J. Fluid Mech.,* **289,** 115–128.